Full Paper

Journal of Agricultural Meteorology 76(1): 1-10, 2020

Observation of vertical profiles of NO, O_3, and VOCs to estimate their sources and sinks by inverse modeling in a Japanese larch forest

Ryuichi WADA[a,†], Masahito UEYAMA[b], Akira TANI[c], Tomoki MOCHIZUKI[c], Yuzo MIYAZAKI[d], Kimitaka KAWAMURA[e], Yoshiyuki TAKAHASHI[f], Nobuko SAIGUSA[f], Satoru TAKANASHI[g], Takafumi MIYAMA[g], Takashi NAKANO[h], Seiichiro YONEMURA[i], Yutaka MATSUMI[j] and Genki KATATA[k]

[a] Department of Natural and Environmental Science, Teikyo University of Science, Uenohara 409-0193, Japan
[b] Graduate School of Life and Environmental Sciences, Osaka Prefecture University, Sakai 599-8531, Japan
[c] Graduate Division of Nutritional and Environmental Sciences, University of Shizuoka, Shizuoka 422-8526, Japan
[d] Institute of Low Temperature Science, Hokkaido University, Sapporo 060-0819, Japan
[e] Chubu Institute for Advanced Studies, Chubu University, Kasugai 487-8501, Japan
[f] National Institute for Environmental Studies, Tsukuba 305-8506, Japan
[g] Forestry and Forest Products Research Institute, Tsukuba 305-8687, Japan
[h] Mount Fuji Research Institute, Fujiyoshida 403-0005, Japan
[i] National Institute for Environmental Studies, NARO, Tsukuba 305-8506, Japan
[j] Institute for Space-Earth Environmental Research, Nagoya University, Nagoya 464-8601, Japan
[k] Institute for Global Change Adaptation Science, Ibaraki University, Mito 310-8512, Japan

Abstract

Trace atmospheric gases in the biosphere, such as ozone (O_3), nitrogen oxides (NO_x), and biogenic volatile organic compounds (BVOCs), can affect the carbon cycle as well as the climate. Vertical profiles of nitric oxide (NO), O_3, and volatile organic compound (VOC) concentrations were measured at a Japanese larch (*Larix kaempferi*) forest in the foothills of Mt. Fuji in Japan over an 11-day period in July 2012. The concentrations of NO and O_3 during the day were highest above the canopy and decreased with proximity to the forest floor, but those of the VOCs had minimum and maximum points at different levels within the canopy depending on the species. Inverse multilayer models were applied to identify vertical sink and source distribution of these gases within the canopy. The model estimated that there was higher O_3 deposition and absorption at the forest floor than in the canopy layer; therefore, the understory was an important O_3 sink within the forest. A strong NO sink was simulated in the trunk space, where loss by reaction with O_3 is expected. The sinks and sources of BVOC as well as their oxidized products are simulated in the canopy layer and the forest floor. The sink and source distribution suggested that VOC transportation from the neighboring forest also affected the vertical sink and source distribution within the canopy.

Key words: BVOC, Forest, Inverse model, Nitrogen oxides, Ozone

1. Introduction

Trace gases such as ozone (O_3) and nitrogen oxides (NO_x) in the biosphere influence forest growth and carbon storage (Ollinger *et al.*, 2002). O_3 results in a reduction of carbon fixation and biomass production (Reich, 1987; Izuta *et al.*, 1999; Watanabe *et al.*, 2015, 2019; Tani *et al.*, 2017), and atmospheric nitrogen deposition can result in increased growth of terrestrial ecosystems (Vitousek and Howarth, 1991). Biogenic volatile organic compounds (BVOCs) generate secondary organic aerosols that can affect the climate by affecting cloud formation (Kanakidou *et al.*, 2005).

Forest ecosystems are also an important sink and source of trace gases and particle matters in the atmosphere (Slemr and Seiler, 1984; Yamaguchi *et al.*, 2019); thus, observations of trace gas fluxes, such as O_3 (Mikkenlsen *et al.*, 2004; Gerosa *et al.*, 2005; Matsuda *et al.*, 2005), NO_x (Rummel *et al.*, 2002; Horii *et al.*, 2004; Farmer *et al.*, 2006), and BVOCs (Guenther and Hills, 1998: Tani *et al.*, 2002: Mochizuki *et al.*, 2015, 2017) in forest ecosystems have been conducted. In forest ecosystems, O_3 removal processes occur through stomatal uptake by plant leaves, deposition on plant canopies and soil surfaces, and depletion via chemical reactions (Kaplan *et al.*, 1988; Gao *et al.*, 1993; Rannik *et al.*, 2009; Wolfe *et al.*, 2011; Fares *et al.*, 2012; Launiainen *et al.*, 2013). O_3, NO_x, and BVOCs are reactive; therefore, production processes, their strengths, and loss by chemical reactions within a canopy are important. Min *et al.* (2014) measured NO and NO_2 concentration profiles and their fluxes above a forest and suggested that a portion of NO_x was converted to higher nitrogen oxides such as nitric acid (HNO_3) via chemical reaction within the canopy. Fuentes *et al.* (2007) measured isoprene concentration profiles and its oxidized species, such as methacrolein (MACR) and methyl vinyl ketone

Received; June 11, 2018
Accepted; September 1, 2019
†Corresponding Author: wada@ntu.ac.jp
DOI: 10.2480/agrmet.D-18-00029

(MVK), and investigated their production rates at several heights within and above a forest using numerical modeling. If the vertical sink and source distribution within a canopy is known, it will deepen the understanding of trace gas dynamics such as those of O_3, NO_x, and BVOCs within a forest. However, knowledge of the sink and source distribution of the trace gases within forest canopies is limited.

Inverse multilayer models are a useful way of evaluating trace gas sink and source distribution within a canopy (Katul and Albertson, 1999; Leuning *et al.*, 2000; Siqueria *et al.*, 2000; Ueyama *et al*., 2014). Through mathematical simulation of flow in and above the canopy, the methods yield vertical gas flux distributions based on concentration profile measurements. Inverse models have an advantage of being able to directly estimate net loss or production because the model has no *a priori* assumptions as in the case of biological processes. There have been few studies conducted to investigate the distributed O_3 flux in a forest canopy (Rannik *et al.*, 2012; Zhou *et al*., 2017). As far as we know, there have been no studies estimating the vertical sink and source distribution of NO and VOCs using inverse multilayer models for applying whole canopies, which consist of the canopy layer, trunk space, and forest floor. We examined the temporal variation in the NO, O_3, and VOCs profiles within and above the canopy, then applied inverse multilayer models (Ueyama *et al.*, 2014) to identify sink and source distributions of NO, O_3, and VOC within the forest canopy. We then inferred the production and loss processes occurring within the canopy from the obtained sink and source distributions.

2. Materials and Methods

2.1 Site

The measurements were conducted at a planted Japanese larch (*Larix kaempferi*) forest in the foothills of Mt. Fuji in Fujiyoshida, Japan (35° 26′ N, 138° 45′ E, and approximately 1050 m above sea level; Takahashi *et al.*, 2015). The research site is located about 7 km southwest of the city center. The site was characterized by uniformly-planted Japanese larch with interspersed evergreen (*Pinus densiflora*) and broadleaf species (*Swida controversa* and *Quercus crispula*). Understory plants, including fern species (*Dryopteris crassirhizoma*), covered the forest floor. The canopy height was approximately 25 m. The average density and basal area of the larch trees were approximately 406 stems ha^{-1} and 36.6 m^2 ha^{-1}, respectively. The leaf area index was estimated at 2.8 m^2 m^{-2} in summer (Takahashi *et al.*, 2015). Two distinct peaks in leaf area density (LAD) were observed at the forest floor between 0 and 3 m owing to the presence of dense understory plants, and at the crown layer between 15 and 20 m. The mean annual temperature observed at this site is 9.5 ℃; the lowest monthly mean air temperature is −1.7 ℃ in January and the highest monthly mean air temperature is 20.5 ℃ in August. The 12-year average annual precipitation is 1793 mm, and monthly precipitation varies between 47 mm in January and 306 mm in September.

2.2 Measurements

We measured NO and O_3 concentrations at the study site over an 11-day period starting in early July 2012. Concentrations of NO were measured using a chemiluminescence NO_x analyzer (Thermo Scientific, 42i-TL) with a flow rate of 2.5 L min^{-1}. Concentrations of NO_2 were also measured with the same NO_x analyzer using the Mo-converted chemiluminescence technique; however, due to chemical interferences with other nitrogen oxide (EANET, 1999), the data was not included. The detection limit and the precision of the NO analyzer were estimated to be 0.017 ppbv and 0.4%, respectively with a 300 sec integration time (1σ). The O_3 concentration was measured using an ultraviolet absorption O_3 analyzer (Thermo Scientific, 49C) with a flow rate of 1.0 L min^{-1}. The detection limit and precision of the O_3 analyzer were 1 ppbv and 1%, respectively, according to the company information.

A schematic diagram of the sampling and measurement methodologies is shown in Fig. 1. The observation tower was 32 m high, and air samples were collected at four heights of 2, 10, 16, and 28 m with a 220-second interval for each level over a period of 15 minutes using PTFE sampling tubes with 0.25-inch inner diameter. To prevent the degradation of O_3 and NO in the presence of NO_2 and sunlight during the sampling of ambient air, the sampling lines were covered with shade sheets. The losses of the NO and O_3 by sampling tubes were evaluated by changing the tube length from 5 to 40 m, which was below the detection limits. Hourly averaged data of air samples were collected by automatically switching two-port solenoid valves in a sample line control system. In order to obtain enough data to average and stabilize the measurement conditions, such as flow rate and pressure, an interval of 220 seconds was chosen. Because of the response time of the analyzers in combination with the sampling lines, up to 150 seconds of O_3 and NO data, collected just after switching the solenoid valves, were discarded.

While the measurements of VOCs used in the current observations have been previously reported (Mochizuki *et al.*, 2015), a general description of the measurement method is also

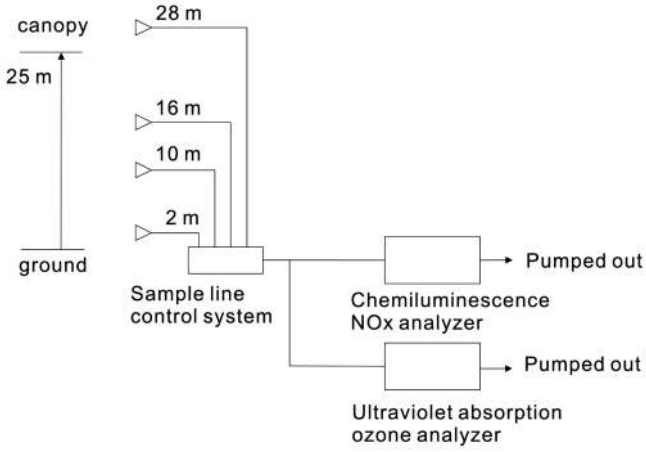

Fig. 1. A schematic diagram of the sampling and observation methodology for NO and O_3. The observation tower was 32 m high and air samples were collected at 220 sec intervals over a period of 15 min at four vertical heights of 2, 10, 16, and 28 m ranging from 2 m above the ground to above the forest canopy. The forest canopy was between 14 m and 25 m. The flow rates of NO_x and O_3 analyzers were 2.5 L min^{-1} and 1.0 L min^{-1}, respectively.

provided. VOC concentrations were measured at five heights of 2, 10, 16, 22, and 28 m on 5, 10, and 15−17 July 2012. Ambient air was collected in stainless steel adsorbent tubes. The tubes were collected every three hours, from 9:00 to 18:00 LT. Isoprene, MACR, MVK, and total monoterpenes (TMT, including α-pinene) were quantified using a gas chromatograph coupled to a mass spectrometer (Shimadzu, QP5050A).

Micrometeorological data, wind speed and direction, solar radiation, precipitation, and air temperature have been continuously recorded at this site.

2.3 Inverse model calculation

To infer vertical distributions of sink and source strength, we used two different inverse models: Lagrangian localized near-field theory (Raupach, 1989) and Eulerian closure model (Katul and Albertson, 1999). The details of the models and parameterizations were reported in Ueyama *et al.* (2014); only a brief description is provided here.

The Lagrangian localized near-field (LNF) theory treats concentrations at a given height i as a superposition of near-field and far-field source or sink contributions. Concentration C at a given layer i is computed as follows:

$$C_i - C_R = \sum_{j=1}^{m} D_{ij} S_j \Delta z_j \quad (1)$$

C_R is the concentration at a reference height (28 m in this study), D_{ij} is the dispersion matrix, S_j is the sink or source strength at layer j, and Δz_j is the depth of the layer j. C_i was calculated as sum of near-field (C_n) and far-field (C_f) contributions. The Lagrangian integral time scale was based on Leuning *et al.* (2000). To calculate C_n and C_f, vertical distributions of turbulent statistics, we used a second order closure model (Wilson and Shaw, 1977).

The Eulerian closure model (EUL) for scalar turbulent transport can be derived as follows:

$$A_1(z)\frac{\partial^2 \overline{w'C'}}{\partial z^2} + A_2(z)\frac{\partial \overline{w'C'}}{\partial z} + A_3(z)\overline{w'C'} = A_4(z) \quad (2)$$

where

$$A_1(z) = \frac{2\tau}{C_8}\overline{w'w'},$$

$$A_2(z) = \frac{\tau}{C_8}\frac{\partial \overline{w'w'}}{\partial z} + 2\frac{\partial}{\partial z}\left(\frac{\tau}{C_8}\overline{w'w'}\right),$$

$$A_3(z) = \frac{\partial}{\partial z}\left(\frac{\tau}{C_8}\frac{\partial \overline{w'w'}}{\partial z}\right) - C_4\frac{1}{\tau},$$

$$A_4(z) = \overline{w'w'}\frac{\partial \overline{C}}{\partial z} - \frac{\partial}{\partial z}\left(\frac{\tau}{C_8}\overline{w'w'w'}\right)\frac{\partial \overline{C}}{\partial z} - \left(\frac{\tau}{C_8}\overline{w'w'w'}\right)\frac{\partial^2 \overline{C}}{\partial z^2} - \frac{4}{3}\frac{g}{\overline{T}}\overline{T'C'}$$

where w is vertical wind velocity, z is height, T is air temperature, g is the gravitational acceleration, τ is the relaxation time scale, and C_4 (2.0) and C_8 (9.0) are closure constants (Siqueira *et al.*, 2000). Overbar and prime represent time average and deviation from time average, respectively. Since the buoyance effect has an important role in scaler transport even within a canopy (Katul *et al.*, 2013), we included the buoyance term in A_4.

The models were validated at the same forest but during different period, in terms of CO_2 and CH_4 fluxes (Ueyama *et al.*, 2014), where the models reasonably inferred diurnal variation, day-by-day variation, and magnitude of the fluxes above the forest during the daytime period.

The model performance during the observational period was examined for CO_2 fluxes. We used the CO_2 concentration profiles and fluxes by the eddy covariance method (Takahashi *et al.*, 2015; Yonemura *et al.*, 2017). The data were applied for calculation when the friction velocity (u^*) was greater than 0.15 ms^{-1}, as the inverse models required sufficient turbulence within the canopy. The observed and calculated CO_2 fluxes of LNF and EUL models from 0:00 on 8 July, 2012 to 24:00 18 July, 2012 (LT) are shown in Fig. 2. Correlations between the observed and calculated CO_2 fluxes are shown from 12:00 9 July to 5:30 15 July (Fig. 3). The regression lines were $F_{CO2\_model} = (0.91 \pm 0.09) \times F_{CO2\_obs} + (2.03 \pm 1.25)$ for LNF and $F_{CO2\_model} = (1.07 \pm 0.08) \times F_{CO2\_obs} + (5.19 \pm 1.06)$ for EUL, respectively. The slopes of the regression lines are 0.91 ± 0.09 and 1.07 ± 0.08, respectively, and they are not significantly different from a unit slope. The correlation coefficients of the regression lines and root mean square error (RMSE) are 0.67 and 16.3 μmol m^{-2} s^{-1} for LNF and 0.81 and 16.4 μmol m^{-2} s^{-1} for EUL, respectively. The model-calculated CO_2 fluxes during a period from 12:00 9 July to 5:30 15 July agreed with the observed CO_2 flux. The inverse model used relative concentrations at each height compared to the concentration above the canopy; therefore, whether the absolute concentrations are high or low does not affect the results of the inverse models. However, if the advection is faster than the time scale of vertical mixing, the model-calculated result might be affected. The

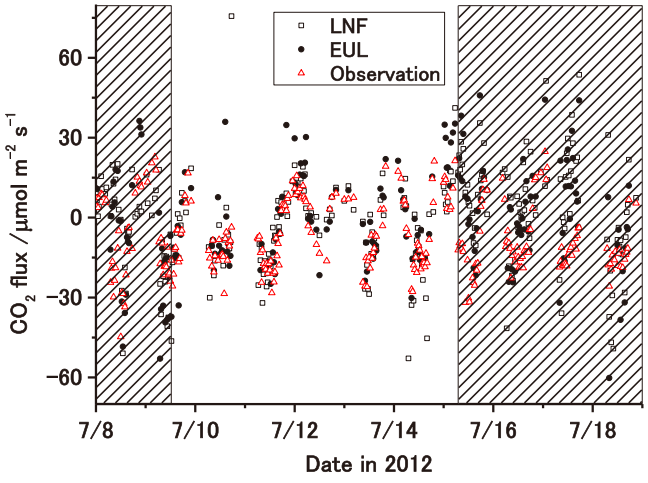

Fig. 2. Observed and calculated CO_2 fluxes using Lagrangian localized near-field theory (LNF) and Eulerian closure model (EUL) from 0:00 on 8 July to 24:00 18 July, 2012 (LT). Data except in the shaded area were used for the correlation plots between the observed and calculated CO_2 fluxes as shown in Fig. 3.

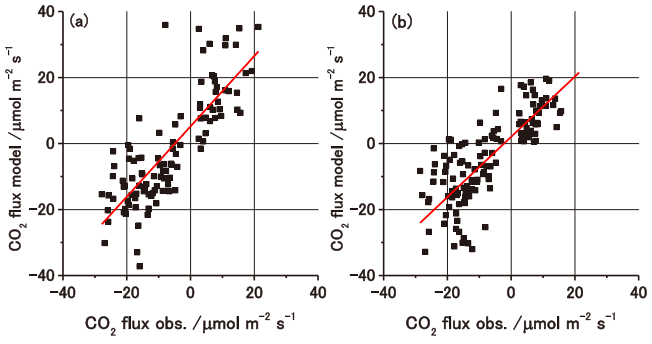

Fig. 3. Scatter plots of the observed and the calculated CO_2 fluxes using the (a) Eulerian closure model (EUL) (b) Lagrangian localized near-field theory (LNF) from 12:00 on 9 July to 5:30 on 15 July, 2012. The regression lines were $F_{CO2\_model} = (0.91 \pm 0.09) \times F_{CO2\_obs} + (2.03 \pm 1.25)$ for LNF and $F_{CO2\_model} = (1.07 \pm 0.08) \times F_{CO2\_obs} + (5.19 \pm 1.06)$ for EUL, respectively. The correlation coefficients of the regression lines and root mean square error (RMSE) are 0.67 and 16.3 μmol m^{-2} s^{-1} for LNF and 0.81 and 16.4 μmol m^{-2} s^{-1} for EUL, respectively.

observed concentration at each height increased overall, including the lower layers within the forest as well as above the canopy, and the calculated CO_2 fluxes also agreed with the observed CO_2 flux during the study period. Therefore, sufficient vertical mixing occurred within the canopy and advection effects could be negligible during the analysis period. The inverse multilayer models were applied to O_3, NO, and VOCs from 12:00 9 July to 5:30 15 July, 2012, when good correlations were obtained between the calculated and observed CO_2 fluxes.

3. Results

3.1 Vertical profiles of O_3, NO, VOCs, and micrometeorological data in the canopy

Figure 4 shows the measured O_3 and NO concentrations and micrometeorological data from 8 to 19 July, 2012. Except 11 to 14 July, the weather during the study period was mostly clear. The prevailing wind direction was from the northeast during the daytime and from the southwest during the nighttime. The average wind speed at 32 m was 1.3 m s^{-1} during the measurement period. The average O_3 and NO concentrations above the canopy were 26.8 and 0.17 ppbv, with maximum concentrations of 71.6 and 0.52 ppbv, respectively. The O_3 concentrations showed a clear diurnal variation with a daytime maximum and nighttime minimum. O_3 is produced

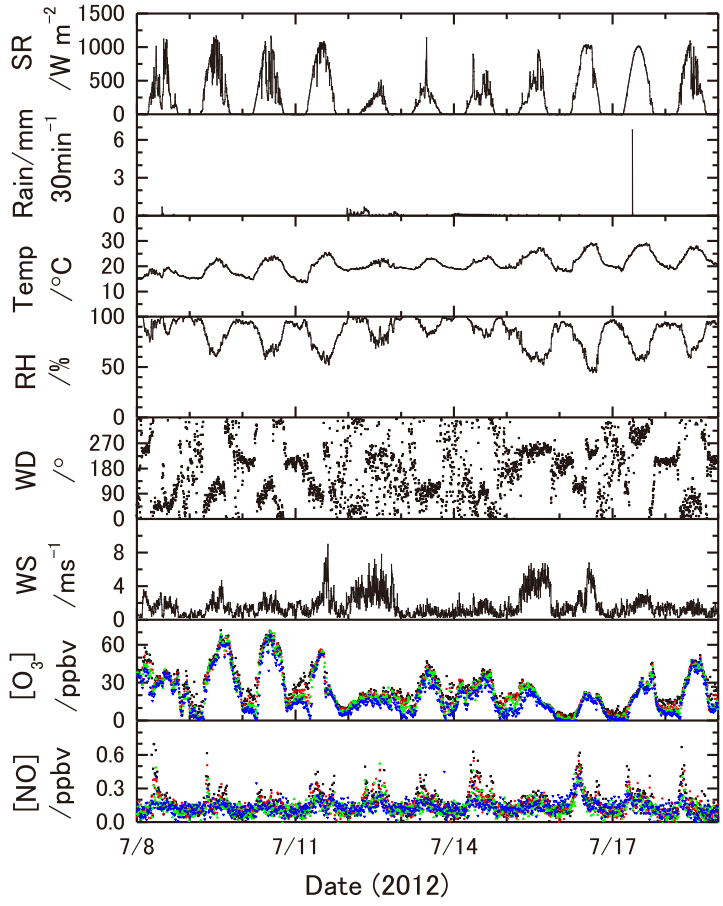

Fig. 4. NO and O_3 concentrations and micrometeorological data from 8 to 19 July, 2012. Micrometeorological data were observed at 32 m. SR is solar radiation, Temp is temperature, RH is relative humidity, WD is wind direction, and WS is wind speed. Colors for gas concentrations indicate variables at different heights: black indicates 28 m, red indicates 16 m, green indicates 10 m, and blue indicates 2 m.

in the atmosphere via photochemical reaction with sunlight (Jacob, 1999). The NO concentrations were sometimes high in the morning because the air mass originating from the city center, which is affected by vehicular emissions, was carried by wind blowing from the northeast from the city center to the mountain site.

Figure 5 shows the LAD and hourly average O_3 and NO concentration profiles during the daytime (10:00–17:00) from 12:00 on 9 July to 5:30 on 15 July, 2012. The data indicate the presence of floor plants on the forest floor from 0 m to 4 m, trunk space from 5 m to 13 m, and a canopy layer from 14 m to 22 m. The O_3 concentration ranged from approximately 30 ppbv to 40 ppbv near the forest floor and from 35 ppbv to 45 ppbv above the canopy. The NO concentration ranged from 0.1 ppbv to 0.2 ppbv at the forest floor and from 0.2 ppbv to 0.3 ppbv above the canopy. Both the O_3 and NO concentrations were highest above the canopy and decreased toward the forest floor within the canopy; however, the rates of decrease differed. The O_3 concentrations largely decreased from 10 m to 2 m, whereas the NO concentrations largely decreased from 28 m to 16 m.

Figure 6 shows the three-hour averaged VOC concentration profiles, including isoprene, TMT, MACR, and MVK during the daytime (9:00–15:00) on 10 July, 2012. The VOC concentration profiles have been previously reported (Mochizuki *et al.*, 2015). However, the profiles and a general description of VOCs have been provided since these data were used in the inverse models. Mochizuki *et al.* (2015) observed VOC concentration profiles on five days (8, 10, 15, 16, and 17 July, 2012) during the observational period; however, only one day of data (10 July, 2012) was used in the inverse models because this day was during a period when good correlations were obtained between the observed and calculated CO_2 fluxes. The isoprene, MACR, MVK, and TMT concentrations ranged from 0.05 to 0.17 ppbv, 0.03 to 0.09 ppbv, 0.04 to 0.10 ppbv, and 0.1 to 0.5 ppbv, respectively. The concentrations of isoprene were the highest at the forest floor and decreased with an increase in height to a minimum concentration at 22 m. The isoprene concentration above the canopy was higher than in the canopy layer. The MACR and MVK concentrations showed similar vertical profiles, with minimum concentrations at 22 m and maximum concentrations at 16 m. The TMT concentration was highest at the forest floor, decreasing with an increase in height.

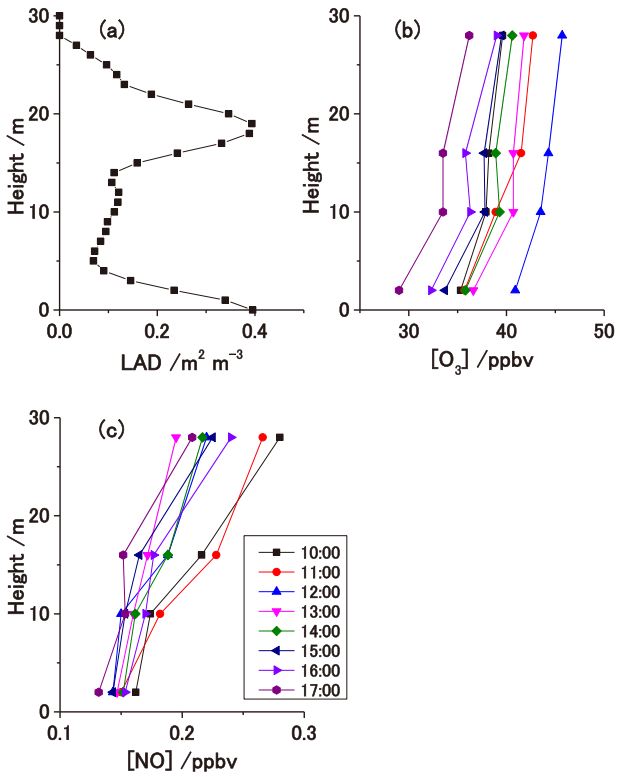

Fig. 5. (a) Leaf area density (LAD; Ueyama *et al.*, 2014) and hourly averaged concentration profiles of (b) O_3 and (c) NO. The concentrations were averaged during a period from 12:00 9 July to 5:30 15 July, 2012, when the observed and the modelled CO_2 fluxes agreed. The times on the figure represent the beginning of the observation time, i.e. 10:00 represents 10:00–11:00.

3.2 Simulated fluxes of the inverse model

The calculated daytime O_3 and NO sink or source distributions showed that the canopy and the forest floor were O_3 sinks during the daytime, except at 11:00 and 12:00 for the canopy, with maximum sinks observed 13:00 (Fig. 7). The trunk space was neither a sink nor a source of O_3. The canopy was estimated to be an NO source, while the trunk space was an NO sink, with the maximum source and sink observed at 14:00. The forest floor was neither a sink nor a source of NO.

The simulated three-hour VOC sink or source distributions during the daytime within the canopy are shown in Fig. 8. The upper and lower canopies were estimated to be isoprene sinks, with the maximum sinks observed at 12:00. The forest floor was estimated as an isoprene source. The trunk space was simulated as an isoprene source at 9:00 and 12:00 but as an isoprene sink at 15:00. Similar variations in sink or source of MACR and MVK were found during the daytime. During the daytime, the upper canopy was a sink of MACR and MVK, whereas the lower canopy was a source. The forest floor and trunk space were not significant sinks or sources of MACR and MVK. The forest floor was an obvious source of TMT, while the upper canopy was a sink. The trunk space and lower canopy were not significant TMT sinks or sources.

Figure 9 shows the daytime-averaged simulated sink or source distributions of EUL and LNF along with the O_3 and NO concentration profiles. In Fig. 9, the vertical sink or source distribution is distinguished by the canopy, trunk space, and forest floor, representing heights of 2, 10, and 16 m, respectively. The daytime-averaged concentration of O_3 showed the highest value above the canopy, and it decreased with height. The daytime-averaged O_3 concentrations in the canopy layer and trunk space were similar. Both models showed that O_3 was consumed at the canopy layer and forest floor, as indicated by the decrease in O_3 concentration at 16 m and 2 m. The O_3 concentration did not change at 10 m, indicating that the trunk space did not include an obvious O_3 sink or source. O_3 is deposited on soils and plant leaves and is absorbed by plants through their stomata (Kaplan *et al.*, 1988). The results indicate that the level of O_3 deposition was approximately two times greater at the forest floor than in the canopy layer. The amount

of O_3 absorbed and deposited in the understory along with the strength of the O_3 sink at the forest floor were large. Considering the high LAD at the forest floor (Fig. 5), the physiology of the understory might play an important role in O_3 absorption and deposition in this forest. The mean values of the storage term of O_3 (dC/dt in Eq. (2)) during the daytime at 16 m (in the canopy layer) and 2 m (at the forest floor) based on the relative concentration above the canopy were 0.005 nmol m^{-3} s^{-1} and 0.002 nmol m^{-3} s^{-1}, respectively. These storage terms were over 100 times smaller than the sinks estimated by the inverse models. Sufficient atmospheric mixing occurred in the forest and the models were not affected by storage of the trace gases during the analysis period of 10:00–17:00.

The daytime-averaged NO concentration was the highest above the canopy and decreased with height (Fig. 9). The concentration in the trunk space was lower than that in the canopy layer, in constant to the concentration profile of O_3. Both models indicated an obvious sink in the trunk space where the

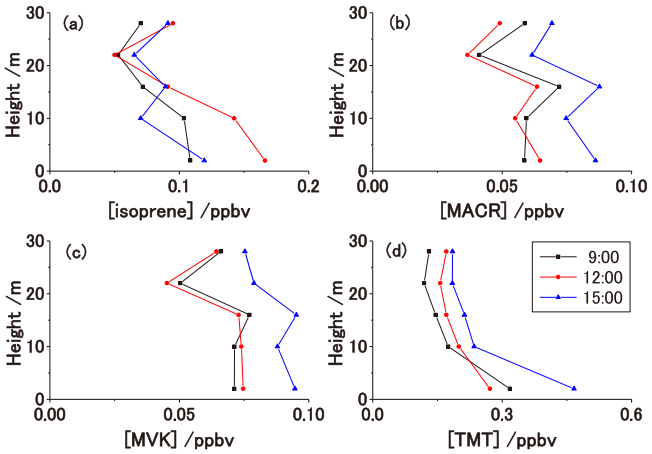

Fig. 6. Concentration profiles of BVOCs including (a) isoprene, (b) methacrolein (MACR), (c) methyl vinyl ketone (MVK) and (d) total monoterpenes (TMT) on 10 July, 2012. The times of 9:00, 12:00 and 15:00 show 9:00–12:00, 12:00–15:00, and 15:00–18:00, respectively.

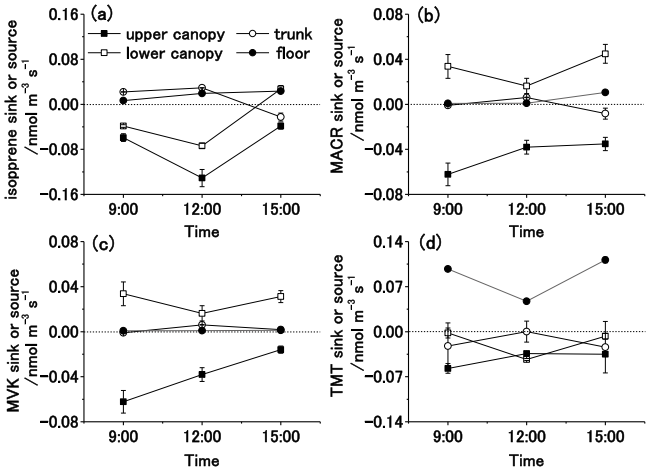

Fig. 8. Calculated sink or source strength of (a) isoprene, (b) methacrolein (MACR), (c) methyl vinyl ketone (MVK), and (d) total monoterpenes (TMT) within a upper canopy and lower canopy layers, trunk space, and forest floor during the daytime using two inverse models on 10 July, 2012. The times of 9:00, 12:00 and 15:00 show 9:00–12:00, 12:00–15:00, and 15:00–18:00, respectively. The sink or source strength are averaged values obtained using the two models, where the error bars represent the highest and lowest values by the two models.

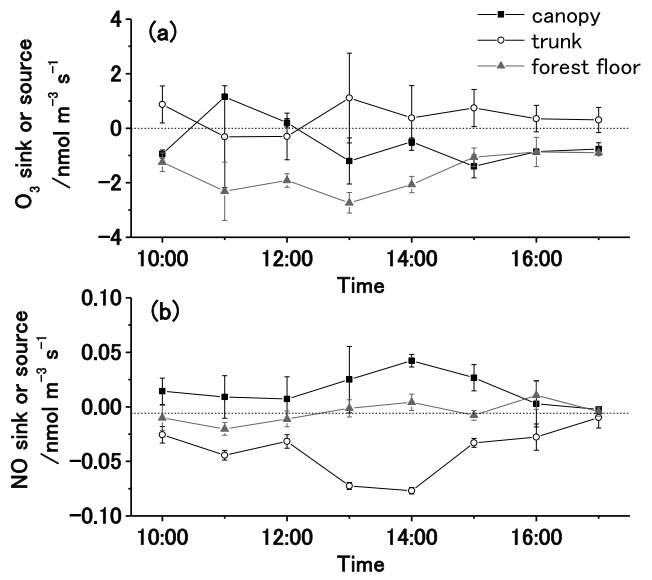

Fig. 7. Calculated hourly averaged sink or source strength of (a) O_3 and (b) NO at the canopy layer, trunk space, and forest floor during the daytime using two inverse models from 9 July to 15 July, 2012. The sink or source strength are averaged values obtained using the two models with the highest and lowest values of error bars corresponding to the calculated values.

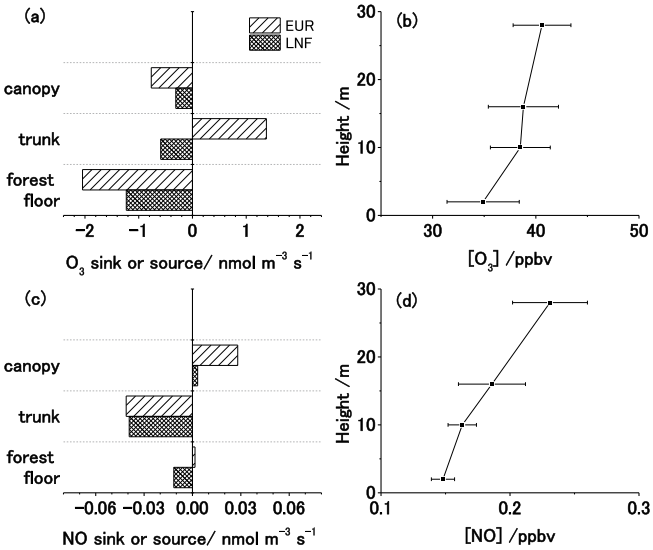

Fig. 9. Daytime-averaged (10:00–17:00) simulated sink/source distribution of (a) O_3 and (c) NO using the Eulerian closure model (EUL) and Lagrangian localized near-field theory (LNF) and concentration profiles for (b) O_3 and (d) NO from 9 July to 15 July, 2012. The vertical distributions are distinguished as the canopy, trunk space, and forest floor, which represent heights of 16 m, 10 m, and 2 m, respectively.

NO concentration decreased. The LNF model indicated an NO sink at the forest floor, whereas the EUL model indicated that the forest floor was a negligible sink or source; the NO concentration decreased at the forest floor. The EUL model indicated an NO source in canopy layer, and the NO concentration decreased at the trunk space.

Figure 10 shows the daytime-averaged simulated VOC vertical sink or source distributions (isoprene, MACR, MVK and TMT) based on the EUL and LNF models, along with the daytime-averaged concentration profiles. The forest floor and trunk space, where the isoprene concentrations were large, were found to be small isoprene sources. The upper and lower canopies were estimated as isoprene sinks; the isoprene concentration was minimized at 22 m, and the concentration at 16 m was lower than that at 10 m. The upper canopy was determined to be a sink of MACR and MVK, which are absorbed by leaves through stomata (Tani *et al.*, 2010, 2013; Karl *et al.*, 2010). The MACR and MVK concentrations showed minimums at 22 m; however, the lower canopy was a source of MACR and MVK and their concentrations were maximized at 16 m. For TMT, the concentration reached its maximum value at 2 m, and the forest floor was a source; TMT is known to be emitted from the soil of coniferous forests (Hayward *et al.*, 2001; Aaltonen *et al.*, 2011; Lin *et al.*, 2007; Miyama *et al.*, 2016).

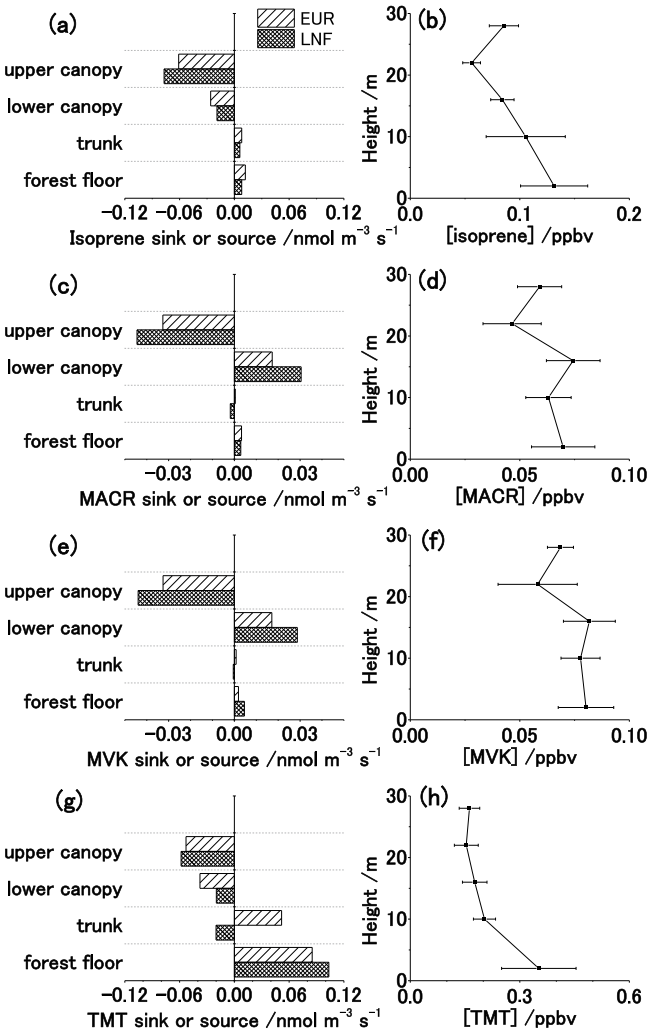

Fig. 10. Daytime-averaged (9:00−18:00) simulated sink or source distribution using the Eulerian closure model (EUL) and Lagrangian localized near-field theory (LNF), and concentration profiles for (a, b) isoprene, (c, d) methacrolein (MACR), (e, f) methyl vinyl ketone (MVK), and (g, h) total monoterpenes (TMT) on 10 July, 2012. The vertical distributions were distinguished as the upper canopy, lower canopy, trunk space, and forest floor, which represent heights of 22 m, 16 m, 10 m, and 2 m, respectively.

The calculated daytime O_3 and NO canopy fluxes (Fig. 11) indicated a downward O_3 flux with a maximum sink at 13:00−14:00. The average daytime O_3 flux (10:00−17:00) during the observation period was −14.1 ± 7.3 nmol m^{-2} s^{-1} for EUL and −14.8 ± 2.7 nmol m^{-2} s^{-1} for LNF, respectively. The range of O_3 flux was similar to previously reported ranges (Kurpius and Goldstein, 2003; Rannik *et al.*, 2009; Zhou *et al.*, 2017). The maximum O_3 flux in a boreal coniferous forest in Finland during August was observed at 14:00, with an average daytime O_3 flux of −7.0 ± 3.4 nmol m^{-2} s^{-1} (Zhou *et al.*, 2017). The daytime NO fluxes (10:00−17:00) were estimated to be −0.11 ± 0.14 nmol m^{-2} s^{-1} for EUL and −0.46 ± 0.26 nmol m^{-2} s^{-1} for LNF, respectively (Fig. 11). The fluxes of isoprene, TMT, MACR and MVK obtained using the inverse models and the relaxed eddy accumulation observation (Mochizuki *et al.*, 2015) on 10 July, 2012 are shown in Fig. 12.

4. Discussion

Because of the limited number of leaves in the trunk space, a plausible explanation for the NO sink at the trunk space (Fig. 9) is that NO was removed through chemical reaction with O_3 as follows:

$$NO + O_3 \rightarrow NO_2 + O_2 \quad (3)$$

NO is generally produced through metabolism and is partly emitted from the soil if it is not processed into other products (e.g., Butterbach-Bahl *et al.*, 2013). However, in this study, no source was estimated at the forest floor (Fig. 9). Even though the soil in this region was immature as previously described, a small amount of NO can be emitted from the soil. The reaction of NO with O_3 also occurs on the forest floor. The sum of the amount of NO emitted from the soil and the amount of NO lost via reaction with O_3 indicated that the forest floor was neither a sink nor source of NO. NO loss also occurs via the reaction with O_3 in the canopy layer; however, the EUL model estimated a source of NO in the canopy layer. One possible explanation is the production of NO via photodissociation of NO_2 by sunlight as follows:

$$NO_2 + h\nu \rightarrow NO + O \quad (\lambda < 420\ \text{nm}) \quad (4)$$

where, h is Planck constant, ν is frequency of light and λ is wavelength.

The average downward solar radiations above the canopy and the forest floor during the daytime (10:00−17:00) were 443 W m^{-2} and 92 W m^{-2}, respectively. The NO_2 photodissociation reaction (Eq. (4)) might be more common in the canopy layer than in the trunk space and forest floor.

However, the trunk space was neither an O_3 sink nor source

(Fig. 9). O_3 reacts stoichiometrically with NO, and the O_3 concentration was over hundred times that of NO. Therefore, the ratio of the loss of O_3 concentration via the reaction between O_3 and NO was less than 1%; it might be difficult to distinguish such a small O_3 sink using the inverse models.

Mochizuki *et al.* (2015) reported that isoprene was emitted from *Dryopteris crassirhizoma* on the forest floor. Isoprene can also be transported from isoprene-emitting *Quercus crispula* in nearby forests (Mochizuki *et al.*, 2014). Thus, the upper canopy was a large sink of isoprene (Fig. 10). Both MACR and MVK are isoprene oxidation products (Tani *et al.*, 2010). The simulated vertical sink or source distributions of MACR and MVK (Fig. 10c, e) suggest that isoprene emitted from floor plants was transported upward and oxidized within the canopy. MACR and MVK were also transported from neighboring forests to the canopy, where they were possibly absorbed by the plant leaves. The inverse models did not estimate MACR and MVK sinks at the forest floor or the trunk space (Fig. 10c, e); the concentrations of MACR and MVK were similar at 2 m and 10 m (Fig. 10d, f), even though they were potentially absorbed by the understory. Even though larch trees emit TMT (Mochizuki *et al.*, 2015), the inverse multilayer models suggested that the upper and lower canopy layers were TMT sinks (Fig. 10g) since the TMT concentration decreased with increasing height from the forest floor (Fig. 10h). TMT is highly reactive and is decomposed in forests with a lifetime of approximately 0.3−0.8 hours (Holzinger *et al.*, 2005). This may explain the loss of TMT emitted from the soil surface.

The estimated NO flux showed a small deposition in the forest (Fig. 11); however, no clear diurnal variations in flux were displayed. Studies of NO emissions from soil (Butterbach-Bahl *et al.*, 2002; Gut *et al.*, 2002) and NO flux measurements upward from the forest floor during the daytime (Horii *et al.*, 2006; Min *et al.*, 2014) have been reported. The simulated NO sink in this study might be explained by the immature surface soil (Takahashi *et al.*, 2015), which can result in lower soil NO emissions. Additionally, NO reacts with O_3 within the canopy to produce NO_2, which can result in the canopy being an NO sink.

The inverse models indicated that isoprene and MACR were deposited in the forest; however, observation suggested that these compounds are emitted (Fig. 12a, c). TMT and MVK were also emitted; however, both models estimated deposition with the exception of at 15:00 (Fig. 12b, d). These discrepancies between the models and observation might be partly explained by an underestimation of the sources of isoprene, MACR, TMT and MVK at the forest floor in the calculation model. Ueyama *et al.* (2014) reported that the wind speeds simulated by the closure model were approximately half the observed values. Since the modeled turbulence at the forest floor was underestimated, the modeled sink and source could be underestimated at the forest floor.

The inverse models show O_3 and NO sinks at the forest floor; however, the O_3 and NO sinks at the forest floor might also be underestimated by the inverse models, as indicated by the VOC result. The total deposition fluxes of O_3 and NO could be possible to be larger than the calculated fluxes.

Only one observational height was set for each characteristic height in the calculation of sink and source distributions in this study. The accuracies of the estimated fluxes can be improved by increasing the number of sampling heights used in concentration measurements (Ueyama *et al.*, 2014).

5. Summary and Conclusions

Over an 11-day period in the beginning of July 2012, NO, O_3, and VOCs (isoprene, MACR, MVK, and TMT) were measured in a larch (*Larix kaempferi*) forest in the foothills of Mt. Fuji in Fujiyoshida, Japan. The distinct sinks and sources of NO, O_3, BVOCs (isoprene and TMT), and oxidation products (MACR

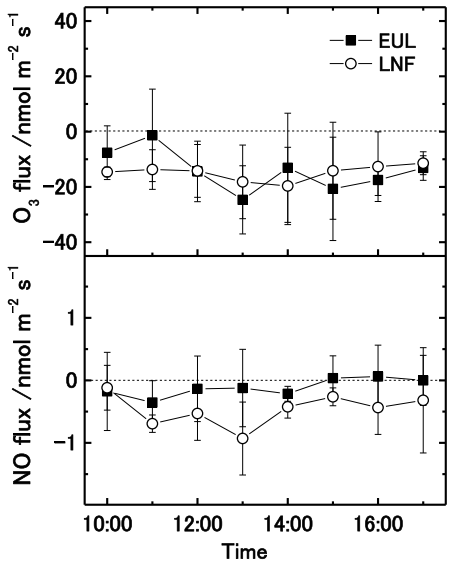

Fig. 11. Hourly averaged total fluxes of O_3 and NO calculated using the two inverse models, Eulerian closure model (EUL) and Lagrangian localized near-field theory (LNF) from 9 July to 15 July, 2012. The error bars show one standard deviation of the means of the calculated fluxes during the observational period.

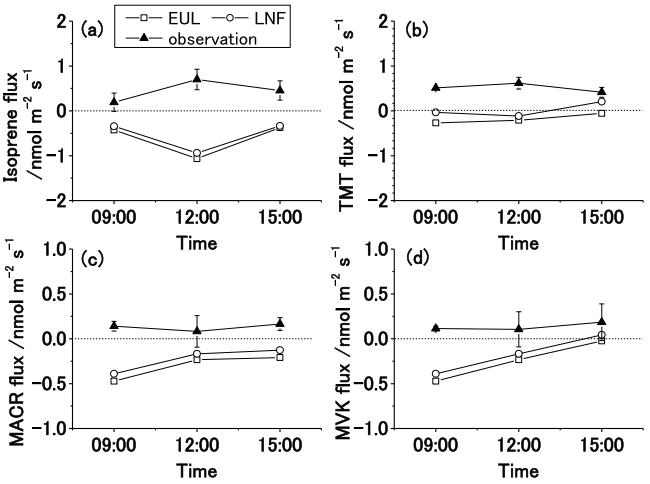

Fig. 12. Total fluxes of (a) isoprene, (b) total monoterpenes (TMT), (c) methacrolein (MACR), and (d) methyl vinyl ketone (MVK) observed (Mochizuki *et al.*, 2015) and calculated using the two inverse models of Eulerian closure model (EUL) and Lagrangian localized near-field theory (LNF) on 10 July, 2012. The times of 9:00, 12:00 and 15:00 show 9:00−12:00, 12:00−15:00, and 15:00−18:00, respectively.

and MVK) within the forest, canopy layer, trunk space, and forest floor were estimated using the inverse multilayer modeling.

The distinct trace gas sinks and sources were explained by absorption, deposition, and emission by the canopy leaves, floor plants, and soil. Higher O_3 deposition and absorption were estimated at the forest floor compared to that in the canopy layer, which suggests that floor plants were important in understanding trace gases dynamics in the forest. The NO sink at the trunk space was mainly caused by a chemical loss reaction with O_3. The inverse models estimated the sinks and sources of the BVOCs and their oxidized products, which could be explained by deposition, absorption, and emission by leaves of the canopy and understory. The inverse models also suggested that the transportation of these species from the neighboring forests also affected the vertical sink and source distribution. This study first showed the possibility to apply the model inversion to estimate the vertical NO and VOC sink and source distribution within a forest canopy.

Acknowledgments

This work was supported by the Grant-in-Aid for Scientific Research (KAKENHI 16K00520) and the Ichimura Foundation for new Technology. The inverse models were developed with a support by Grant-in-Aid for Scientific Research (KAKENHI 23681004 and 26701002).

References

Aaltonen H, Pumpanen J, Pihlatie M, Hakola H, Hellen H, Kulmala L, Vesala T, Back J, 2011: Boreal pine forest floor biogenic volatile organic compound emissions peak in early summer and autumn. *Agricultural and Forest Meteorology* **151**, 682–691.

Butterbach-Bahl K, Breuer L, Gasche R, Willibald G, Papen H, 2002: Exchange of trace gases between soils and the atmosphere in Scots pine forest ecosystems of the northern German lowlands 1. Fluxes of N_2O, NO/NO_2 and CH_4 at forest sites with different N-deposition, *Forest Ecology and Management* **167**, 123–134.

Butterbach-Bahl K, Baggs EM, Dannenmann M, Kiese R, Zechmeister-Boltenstern S, 2013: Nitrous oxide emissions from soils: how well do we understand the processes and their controls? *Philosophical Transactions of Royal Society B* **368**, 20130122.

Fares S, Weber R, Park JH, Gentner D, Karlik J, Goldstein AH, 2012: Ozone deposition to an orange orchard: Partitioning between stomatal and non-stomatal sinks. *Environmental Pollution* **169**, 258–266.

Farmer DK, Wooldridge PJ, Cohen R, 2006: Application of thermal-dissociation laser induced fluorescence (TD-LIF) to measurement of HNO_3, Σalkyl nitrates, Σperoxy nitrates, and NO_2 fluxes using eddy covariance. *Atmospheric Chemistry and Physics* **6**, 3471–3486.

Fuentes JD, Wand D, Bowling DR, Potosnak M, Monson RK, Goliff WS, Stockwell WR, 2007: Biogenic hydrocarbon chemistry within and above a mixed deciduous forest. *Journal of Atmospheric Chemistry* **56**, 165–185.

Gao W, Wesely ML, Doskey PV, 1993: Numerical modeling of the turbulent diffusion and chemistry of NO_x, O_3, isoprene, and other reactive trace gases in and above a forest canopy. *Journal of Geophysical research* **98**, 18339–18353.

Gerosa G, Vitale M, Finco A, Manes F, Denti AB, Cieslik S, 2005: Ozone uptake by an evergreen Mediterranean forest (*Quercus ilex*) in Italy. *Atmospheric Environment* **39**, 3255–3266.

Guenther AB and Hills AJ, 1998: Eddy covariance measurement of isoprene fluxes. *Journal of Geophysical Research* **103**, 13145–13152.

Gut A, van Dijk SM, Scheibe M, Rummel U, Welling M, Ammann C, Meixner FX, Kirkman GA, Andreae MO, Lehmann BE, 2002: NO emission from an Amazonian rain forest soil: Continuous measurements of NO flux and soil concentration. *Journal of Geophysical Research: Atmospheres* **107**, doi: 10.1029/2001JD000521.

Hayward S, Muncey RJ, James AE, Halsall CJ, Hewitt CN, 2001: Monoterpene emissions from soil in a Sitka spruce forest. *Atmospheric Environment* **35**, 4081–4087.

Holzinger R, Lee A, Paw UKT, Goldstein AH, 2005: Observations of oxidation products above a forest imply biogenic emissions of very reactive compounds. *Atmospheric Chemistry and Physics* **5**, 67–75.

Horii MZ, Munger JW, Wofsy SC, Zahniser M, Nelson D, McManus JB, 2004: Fluxes of nitrogen oxides over a temperate deciduous forest. *Journal of Geophysical Research* **109**, doi: 10.1029/2003JD004326.

Horii CV, Munger JW, Wofsy AC, Zahniser M, Nelson D, McManus JB, 2006: Atmospheric reactive nitrogen concentration and flux budgets at a Northeastern U.S. forest site. *Agricultural and Forest Meteorology* **136**, 159–174.

Izuta T, Takahashi K, Matsumura H, Totsuka T, 1999: Cultivar difference of *Brassica campestris* L. in the sensitivity to O_3 based on the dry weight growth. *Journal of Japan Society for Atmospheric Environment* **34**, 145–154.

Jacob DJ, 1999: *Introduction to Atmospheric Chemistry*, Princeton University Press, New Jersey, pp. 266.

Kanakidou K, Seinfeld JH, Pandis SN, Barnes I, Dentener FJ, Facchini MC, Van Dingene R, Ervens B, Nenes A, Nielsen CJ, Swietlicki E, Putaud JP, Balkanski Y, Fuzzi S, Horth J, Moortgat GK, Winterhalter R, Myhre CEL, Tsigaridis K, Vignati E, Stephanou EG, Wilson J, 2005: Organic aerosol and global climate modeling: a review. *Atmospheric Chemistry and Physics* **5**, 1053–1123.

Kaplan WA, Wofsy SC, Keller M, Costa JMD, 1988: Emission of NO and deposition of O_3 in a tropical forest system. *Journal of Geophysical Research* **93**, 1389–1395.

Karl T, Harley P, Emmons L, Thornton B, Guenther A, Basu C, Turnipseed A, Jardine K, 2010: Efficient atmospheric cleansing of oxidized organic trace gases by vegetation. *Science* **330**, 816–819.

Katul GG, Albertson JD, 1999: Modeling CO_2 sources, sinks, and fluxes within a forest canopy. *Journal of Geophysical Research* **104**, 6081–6091.

Katul GG, Cava D, Siqueira M, Poggi D, 2013: Scalar turbulence within the canopy sublayer. In *Coherent Flow Structures at Earth's Surface* (ed. by Venditti JG, Best JL, Church M, Hardy RJ). John Wiley and Sons, New Jersey, pp. 73–95.

Kurpius MR, Goldstein AH, 2003: Gas-phase chemistry dominates O_3 loss to a forest, implying a source of aerosols and hydroxyl radicals to the atmosphere. *Geophysical Research Letters* **30**, 1371–1375.

Launiainen S, Katul GG, Gronholm T, Vesala T, 2013: Partitioning ozone fluxes between canopy and forest floor by measurements and a multi-layer model. *Agricultural and Forest Meteorology* **173**, 85–99.

Leuning RO, Denmead T, Miyata A, Kim J, 2000: Source/sink distributions of heat, water vapor, carbon dioxide and methane in a rice canopy estimated using Lagrangian dispersion analysis. *Agricultural and Forest Meteorology* **104**, 233-249.

Lin C, Owen SM, Penuelas J, 2007: Volatile organic compounds in the roots and rhizosphere of *Pinus* spp. *Soil Biology & Biochemistry* **39**, 951-960.

Matsuda K, Watanabe I, Wingpud V, Theramongkol P, Khummongkol P, Wangwongwatana S, Totsuka T, 2005: Ozone dry deposition above a tropical forest in the dry season in northern Thailand. *Atmospheric Environment* **39**, 2571-2577.

Mikkelsen TN, Ro-Poulsen H, Hovmand MF, Jensen NO, Pilegaard K, Egelov AH, 2004: Five-year measurements of ozone fluxes to a Danish Norway spruce canopy. *Atmospheric Environment* **38**, 2361-2371.

Min KE, Pusede SE, Browne EC, LaFranchi BW, Wooldridge PJ, Cohen RC, 2014: Eddy covariance fluxes and vertical concentration gradient measurements of NO and NO_2 over a ponderosa pine ecosystem: observational evidence for within-canopy chemical removal of NO_x. *Atmospheric Chemistry and Physics* **14**, 5495-5512.

Miyama T, Morishita T, Okumura M, Miyashita S, Takanashi S, Yoshifuji N, 2016: Spatial variations in α-pinen emissions from soils in a red pine forest. *Journal of the Japanese Forest* **98**, 59-64.

Mochizuki T, Tani A, Takahashi Y, Saigusa N, Ueyama M, 2014: Long-term measurement of terpenoid flux above a Larix kaempferi forest using a relaxed eddy accumulation. *Atmospheric Environment* **83**, 53-61.

Mochizuki T, Miyazaki Y, Ono K, Wada R, Takahashi Y, Saigusa N, Kawamura K, Tani A, 2015: Emissions of biogenic volatile organic compounds and subsequent formation of secondary organic aerosols in a *Larix kaempferi* forest. *Atmospheric Chemistry and Physics* **15**, 12029-12041.

Mochizuki T, Kawamura K, Miyazaki Y, Wada R, Takahashi Y, Saigusa N, Tani A, 2017: Secondary formation of oxalic acid and related organic species from biogenic sources in a larch forest at the northern slope of Mt. Fuji. *Atmospheric Environment* **166**, 255-262.

Ollinger S, Aber JD, Reich PB, Freuder RJ, 2002: Interactive effects of nitrogen deposition, tropospheric ozone, elevated CO_2 and land use history on the carbon dynamic of northern hardwood forests. *Global Change Biology* **8**, 545-562.

Rannik Ü, Mammarella I, Keronen P, Vesala T, 2009: Vertical advection and nocturnal deposition of ozone over a boreal pine forest. *Atmospheric Chemistry and Physics* **9**, 2089-2095.

Rannik Ü, Altimir N, Mammarella I, Bäck J, Rinne J, Ruuskanen TM, Hari P, Vesala T, Kulmala M, 2012: Ozone deposition into a boreal forest over a decade of observations: evaluationg deposition partitioning and driving variables. *Atmospheric Chemistry and Physics* **12**, 12165-12182.

Raupach MR, 1989: Applying Lagrangian fluid mechanics to infer scalar source distributions from concentration profiles in plant canopies. *Agricultural and Forest Meteorology* **47**, 85-108.

Reich PB, 1987: Quantifying plant response to ozone: a unifying theory. *Tree Physiology* **3**, 63-91.

Rummel U, Ammann C, Gut A, Meixner FX, Andreae MO, 2002: Eddy covariance measurements of nitric oxide flux within an Amazonian rain forest. *Journal of Geophysical Research* **107**, doi: 10.1029/2001JD000520.

Siqueira M, Lai CT, Katul G, 2000: Estimating scalar sources, sinks, and fluxes in a forest canopy using Lagrangian, Eulerian, and hybrid inverse models. *Journal of Geophysical Research* **105**, 29475-29488.

Slemr F and Seiler W, 1984: Field measurements of NO and NO_2 emissions from fertilized and unfertilized soils. *Journal of Atmospheric Chemistry* **2**, 1-24.

Takahashi Y, Saigusa N, Hirata R, Ide R, Fujinuma Y, Okano T, Arase T, 2015: Characteristics of temporal variations in ecosystem CO_2 exchange in a temperate deciduous needle-leaf forest in the foothills of a high mountain. *Journal of Agricultural Meteorology* **71**, 302-317.

Tani A, Nozoe S, Aoki M, Hewitt CN, 2002: Monoterpene fluxes measured above a Japanese red pine forest at Oshiba plateau, Japan. *Atmospheric Environment* **36**, 3391-3402.

Tani A, Tobe S, Shimizu S, 2010: Uptake of methacrolein and methyl vinyl ketone by tree saplings and implications for forest atmosphere. *Environmental Science & Technology* **44**, 7096-7101.

Tani A, Tobe S, Shimizu S, 2013: Leaf uptake of methyl ethyl ketone and croton aldehyde by Castanopsis sieboldii and Viburnum odoratissimum saplings. *Atmospheric Environment* **70**, 300-306.

Tani A, Ohno T, Saito T, Ito S, Yonekura T, Miwa M, 2017: Effects of ozone on isoprene emission from two major *Quercus* species native to East Asia. *Journal of Agricultural Meteorology* **73**, 140-145.

Ueyama M, Takanashi S, Takahashi Y, 2014: Inferring methane fluxes at a larch forest using Lagrangian, Eulerian, and hybrid inverse models. *Journal of Geophysical Research: Biogeosciences* **119**, doi: 10.1002/2014JG002716.

Vitousek PM, Howarth RW, 1991: Nitrogen limitation on land and in the sea: How can it occur? *Biogeochemistry* **13**, 87-115.

Watanabe M, Hoshika Y, Inada N, Koike T, 2015: Difference in photosynthetic responses to free air ozone fumigation between upper and lower canopy leaves of Japanese oak (*Quercus mongolica* var. *crispula*) saplings. *Journal of Agricultural Meteorology* **71**, 227-231.

Watanabe M, Okabe S, Kinose Y, Hiroshima H, Izuta T, 2019: Effects of ozone on soil respiration rate of Siebold's beech seedlings grown under different soil nutrient conditions. *Journal of Agricultural Meteorology* **75**, 39-46.

Wilson NR, Shaw RH, 1977: A high order closure model for canopy flow. *Journal of Applied Meteorol*ogy **16**, 1198-1205.

Wolfe GM, Thornton JA, McKay M, Goldstein AH, 2011: Forest-atmosphere exchange of ozone: sensitivity to very reactive biogenic BVOC emissions and implications for in canopy photochemistry. *Atmospheric Chemistry and Physics* **11**, 7875-7891.

Yamaguchi M, Tsuji S, Ogata K, Ide H, Matsushita T, Murao N, 2019: Deposition of long-rage transported particle matter on the needle surfaces of Japanese cypress (*Chamaecyparis obtusa*) grown in Nagasaki located in the western region of Japan. *Journal of Agricultural Meteorology* **75**, 30-38.

Yonemura S, Ono K, Ikawa H, Kim W, Mano M, Miyata A, 2017: Comparison of fallow season CO_2 efflux from paddy soil estimated using laboratory incubation with eddy covariance-based flux. *Journal of Agricultural Meteorology* **73**, 140-145.

Zhou P, Ganzeveld L, Rannik U, Zhou L, Gierens R, Taipale D, Mammarella I, Boy M, 2017: Simulating ozone dry deposition at a boreal forest with a multi-layer canopy deposition model. *Atmospheric Chemistry and Physics* **17**, 1361-1379.